Chapter X

RADIATION SHIELDING

M.A. ABDOU — USA
G. CASINI — Euratom
T. HIRAOKA — Japan
G.E. SHATALOV — USSR

Radiation shielding is assessed in this chapter mainly from the nuclear point of view, i.e. to define the optimum thicknesses and the optimized combination of shield materials and to characterize the nuclear performance of the INTOR components. The engineering aspects of the shield system are discussed in Section IV-4.

1. GENERAL DESCRIPTION OF SHIELD CONFIGURATIONS

The INTOR shield system consists of the torus bulk shield, which surrounds the torus structure of the blanket, and various penetration shields, which prevent radiation streaming through openings in the torus structure such as neutral beam injector ports and divertor channels. The bulk shield is divided into two major regions, the inboard bulk shield and the outboard bulk shield, as shown schematically in Fig. X-1. The reactor building walls also serve as biological shield.

The inboard shield is mainly for shielding the central part of the superconducting magnet system. The outboard shield is designed for radiation protection of reactor components such as magnets and to satisfy the criteria for personnel access.

The top and bottom shields must have essentially the same nuclear characteristics as the outboard shield and they will be discussed under this title.

The total thickness of the inboard shield is 85 cm, out of a 1.1 m total distance from the surface of the first wall to the inner surface of the conductor region of the toroidal field coil. These dimensions include gaps, dewars and insulation other than the actual shielding.

The reference configuration of the inboard shield consists of a removable region of about 40 cm thickness, with 90% Type 316 stainless steel and 10% H_2O, and a semi-permanent region of about 30 cm thickness, with 60% boron steel and 40% H_2O. Neutron absorption in the second region can also be accomplished when the borated steel is replaced by B_4C and steel.

The total thickness of the outboard blanket/shield region is 1.65 m, which includes a 50 cm blanket region, a 10 cm gap between the blanket region and the

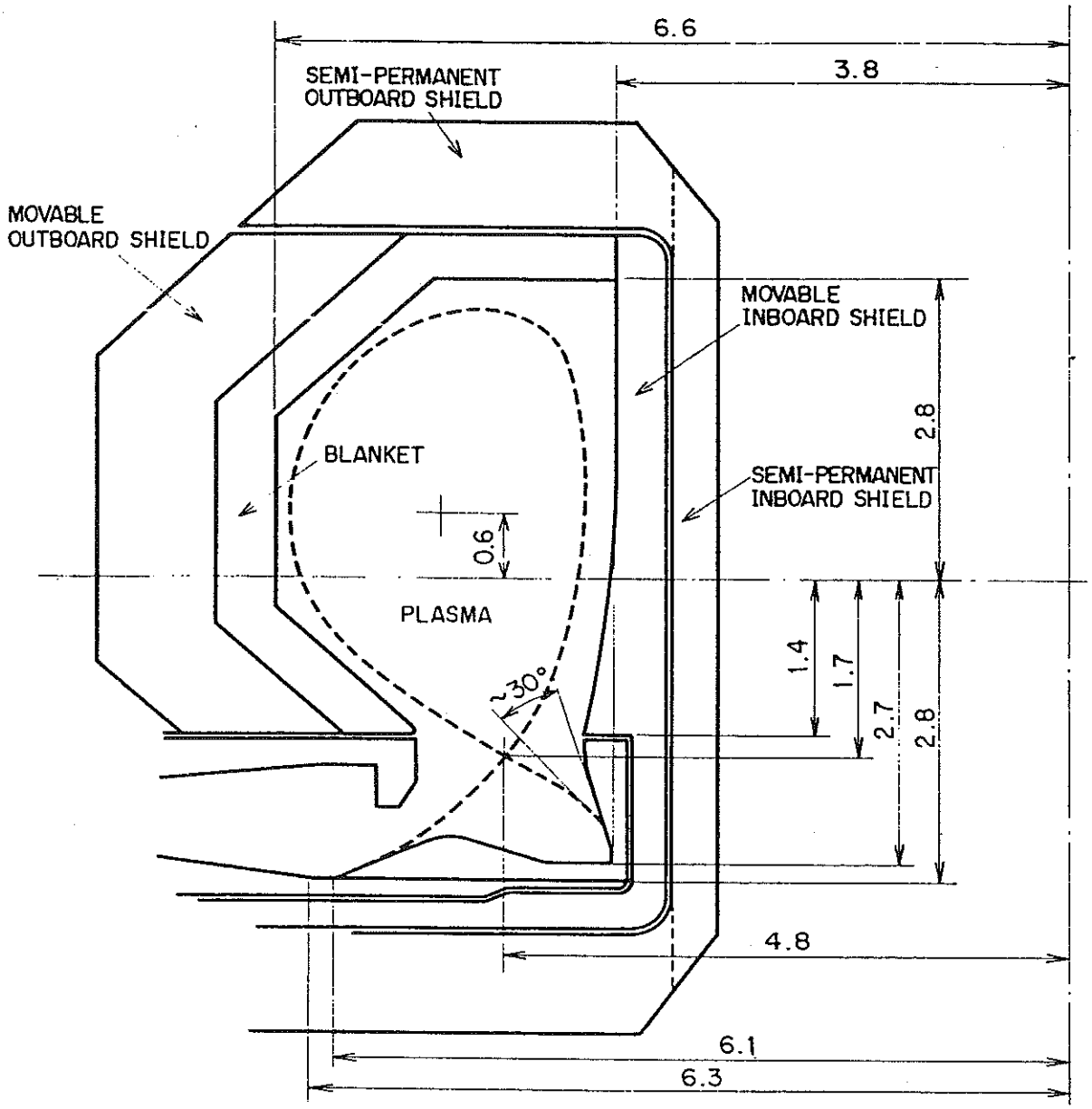

FIG.X-1. Schematic configuration of the shield. (Dimensions in metres)

shield region, and a 105 cm bulk shield. The first region of the outboard shield (closest to the blanket region) will be composed of 90% steel and 10% water. Its thickness will be about 70 cm. The neutron absorption region, with boron steel and water or low-nickel steel and B_4C, will be about 25 cm thick. B_4C can be used instead of boron in the steel. The outermost layer is a 4-cm-thick region of lead. Low-nickel steel is preferable for the outboard shield in reducing induced radioactivity.

TABLE X-1. MAJOR PENETRATIONS OF THE VACUUM VESSEL

	Size	Number
Neutral beam injection port	1 m × 1.2 m	6
Divertor port	0.5 m × 1.3 m	12
Others		
diagnostics ports		
test channels		
test modules		

The semi-permanent top and bottom shields have the same shield dimensions and material compositions as the outboard shield.

The vacuum vessel has many openings that require penetration shields. The major penetrations are listed in Table X-1. The required penetration shields for the neutral beam injector port and the divertor ducts (see Table X-2) have the following thicknesses:

Neutral beam drift tubes	100 cm
Surface of the beam injector box facing the drift tube	75 cm
Rest of the neutral beam system	50 cm
Divertor duct	50 cm

2. GENERAL CONSIDERATIONS

The objective of the bulk shield is to provide sufficient neutron and gamma-ray attenuation to protect reactor components, plant operators and the general public from inacceptable radiation levels at all times during operation, shut-down and off-normal conditions. An important requirement adopted in INTOR is to allow reactor accessibility for maintenance during shut-down periods. This requirement was the main consideration for many aspects of the shield design.

TABLE X-2. PENETRATION SHIELD PARAMETERS USED IN THE THREE-DIMENSIONAL SHIELDING ANALYSIS FOR THE INTOR NEUTRAL BEAM INJECTOR AND DIVERTOR DESIGN

Zone	Zone thickness (cm)	Zone composition (vol.%)	
First wall	1	70%	Type 316 SS
		30%	H_2O
Fe-B shield	45	70%	Fe-1422 alloy
		10%	H_2O
		18%	B_4C
		2%	Void
Pb shield	4	100%	Pb

2.1. Design criteria for superconducting coils

Since the toroidal field (TF) coils are located closer to the reactor plasma than the poloidal field coils, the design criteria for the TF coils are more demanding. These criteria are:

(a) Maximum nuclear heating of 5 kW in the TF coils
(b) Maximum tolerable dose of 10^{10} rad in the insulator materials at the end of life (6 MW·a/m^2)
(c) Maximum neutron fluence of 10^{18} n/cm^2 ($E > 0.1$ MeV) in the superconductor material (Nb_3Sn) at the end of life
(d) Maximum induced resistivity of 5×10^{-8} $\Omega \cdot$cm in the copper stabilizer at the end of life.

Of these criteria, the third one is least limiting. The permissible neutron fluences are listed in Table X-3.

2.2. Personnel access

During the INTOR Phase-Zero studies it was decided that the radiation shield should be designed to permit personnel access during shut-down periods. Personnel access allows some maintenance operations in the reactor building (outside the

TABLE X-3. PERMISSIBLE NEUTRON FLUENCE OF SUPERCONDUCTING COILS ($E_n > 0.1$ MeV)

Material	Changing parameter	Permissible neutron fluence (n/m^2) $E > 0.1$ MeV
NbTi	Critical current	$(0.5-3) \times 10^{19}$
Nb_3Sn		$(1-3) \times 10^{18}$
Epoxy insulation	Breakdown resistance	$(0.5-1) \times 10^{18}$
Stabilizer (Cu)	Resistivity	5×10^{17}

bulk shield) to be performed in direct contact or in a semi-remote mode. This reduces the maintenance down-time considerably. Therefore, the shield design and materials selected for components in the outer periphery of the reactor have to ensure that the biological dose rate in the reactor building is sufficiently low to permit maintenance operators to enter the reactor building within a reasonably short time after reactor shut-down. The specific criterion adopted at present is that the biological dose rate outside the bulk shield, with all shielding in place, must be < 2.5 mrem/h within 24 hours after shut-down.

2.3. General design principles

The following principles have been applied to shield design:

(a) Reduction of high-energy neutrons (> 0.1 MeV) to minimize threshold reactions such as (n, p) (n, α) and (n, 2n) which generate long-lived radioisotopes
(b) Use of material with low-activation cross-sections, especially in the outer region of the shield
(c) Use of neutron absorption material in the thermalization region
(d) Application of an effective gamma shield material (lead) at the outboard shield
(e) No use of expensive or exotic material such as tungsten.

2.4. Neutron source distribution

The average 14 MeV neutron flux density at the first wall corresponding to a neutron wall loading of 1.3 MW/m^2 is 5.8×10^{13} $n/cm^2 \cdot s$. The corresponding

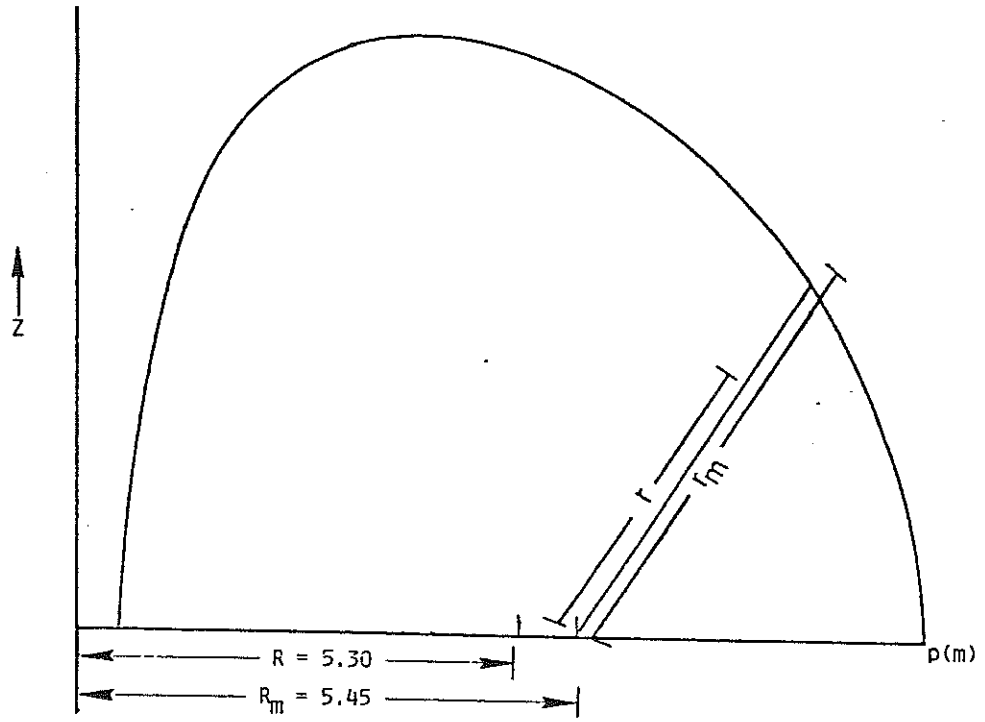

FIG.X-2. Plasma boundary.

total neutron flux density (0 to 14 MeV) is $\sim 5 \times 10^{14}$ n/cm$^2 \cdot$s; however, this varies somewhat with the specifics of the design [6].

The spatial distribution of neutron sources used in the three-dimensional Monte-Carlo calculations and in determining the spatial distribution of the wall loading is described below. The neutron source distribution N(r, z, E) is given by:

$$N(r, z, E) = S(r, z) \cdot n(E)$$

where S(r, z) represents the spatial distribution and n(E) the energy spectrum.

The spatial distribution is based on fusion power density and is defined as follows:

$$S(r, z) = [1 - (r/r_m)^2]^2$$

where r and r_m are measured on the magnetic axis, as shown in Fig. X-2.

The plasma boundary is fitted to a D-shape, defined as follows:

$$z = a_0 k \sin t$$

$$\rho = R_0 + a_0 \cos (t + 0.27 \sin t)$$

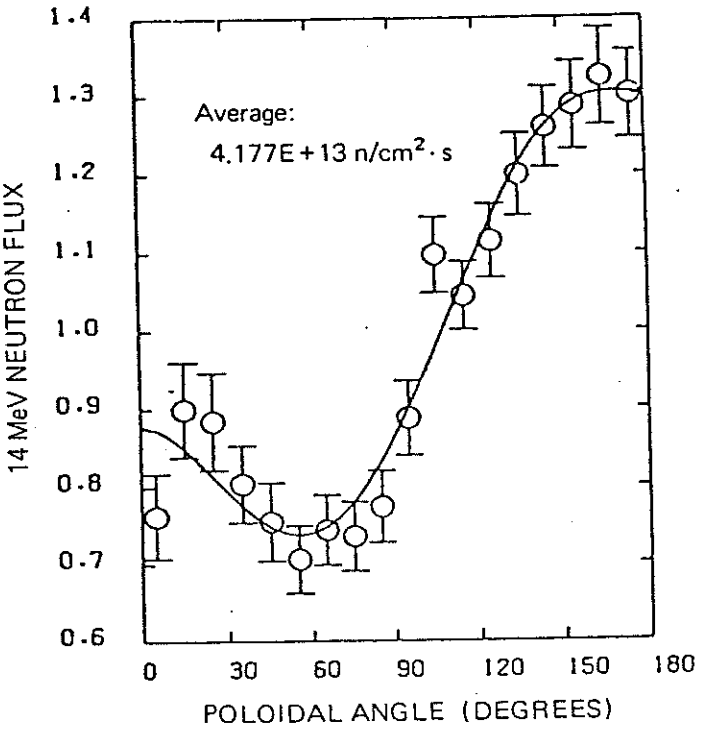

FIG.X-3. Poloidal distribution of 14 MeV neutron flux in the first wall.

where (ρ, z) describes a point on the plasma boundary, t is a parameter which varies from 0 to 180°, a_0 is plasma radius, K is plasma elongation and R is plasma major radius (see Table X-8).

The energy spectrum of the source neutrons from the D-T plasma is:

$$n(E) = \exp\left[-\left(\frac{E-b}{a}\right)^2\right]$$

b = 14.057 MeV
a = 0.3359 MeV

The wall loading has been calculated by Monte-Carlo calculations. It has two peaks at both sides of the mid-plane on the outboard, as shown in Fig. X-3.

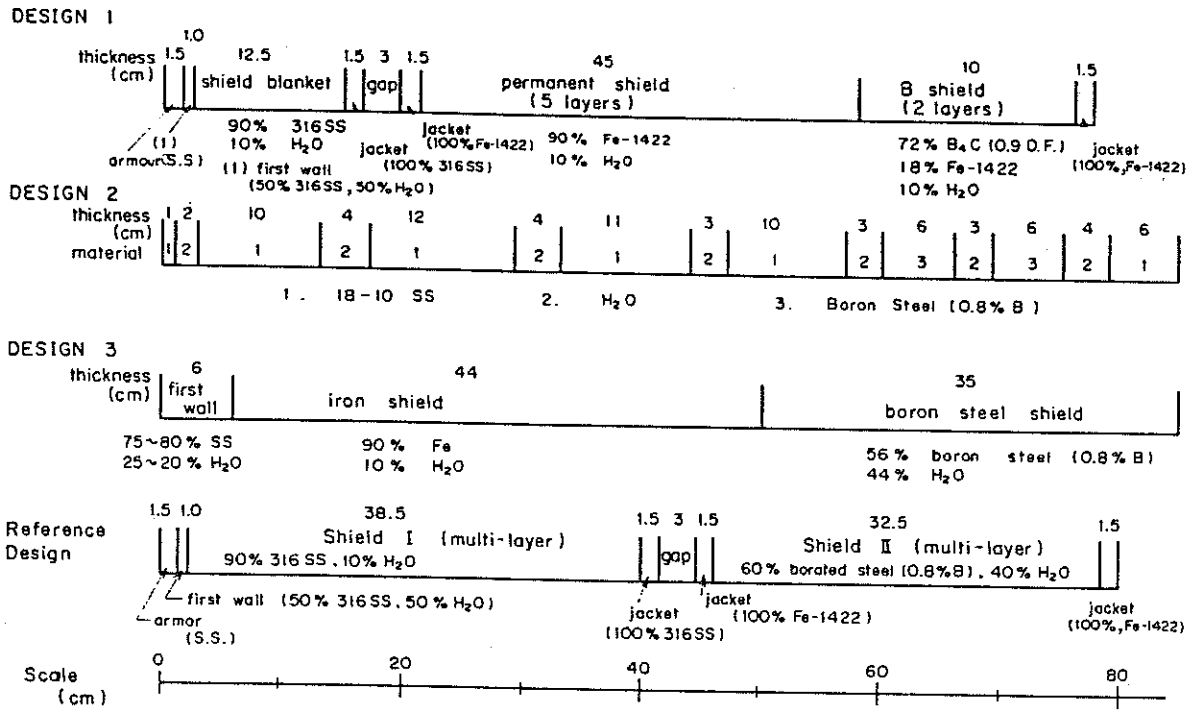

FIG.X-4. Comparison of design options for inboard shield configuration. (Dimensions in cm)

3. TORUS BULK SHIELD

3.1. Inboard bulk shield

3.1.1. Shield configuration

Three design options using no expensive material were investigated (see Fig. X-4). A multi-layer structure of stainless steel (90%) and H_2O (10%) is used in three configurations in the high neutron energy region closest to the blanket. Boron in some form is used in the outer region.

In Option 1 [4], Type 316 stainless steel is utilized for the first wall and the removable portion (so-called shield blanket). The semi-permanent portion of the shield employs Fe-1422 [7] and boron carbide materials. Fe-1422 has the advantage of low nickel and chromium content as compared with other steel types (Types 316 and 304). The lower nickel content results in less long-term radioactivity.

The Fe-1422 steel is a recently developed material with low magnetic permeability in spite of its low nickel and chromium content (~ 2% maximum); it should be noted that Fe-1422 contains 14% manganese. The relatively high corrosion rate of Fe-1422 due to the low chromium content causes concern.

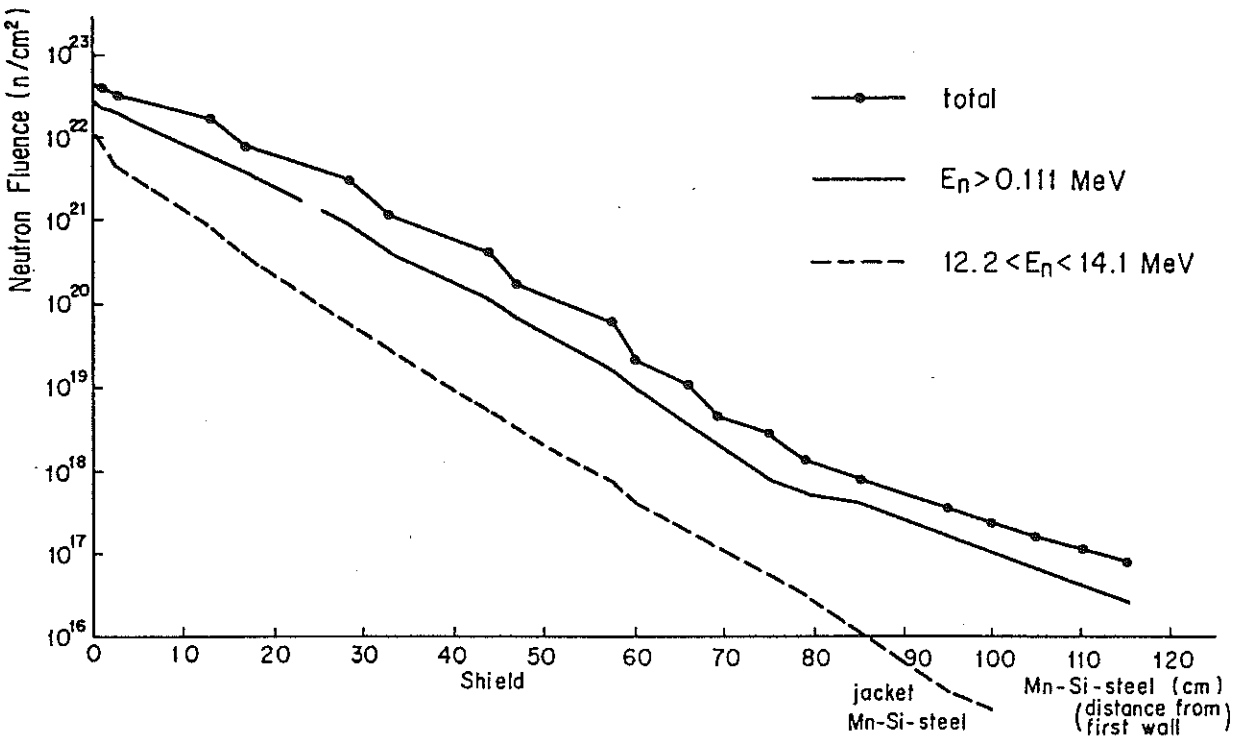

FIG.X-5. Spatial distribution of neutron fluences (inboard shield).

However, this problem is expected to be significantly alleviated by using a small amount of a more conventional corrosion-resistant steel together with Fe-1422. The use of Fe-1422 is very attractive with respect to reactor activation, as already identified in an in-depth study in Refs [8, 9].

Boron carbide with a density factor of 0.9 is used to reduce the fabrication cost by avoiding the need for thermal sintering.

In Options 2 [5] and 3 [2], a mixture of boron steel (0.8% boron) and water is used in the outer region of the shield where a significant fraction of neutrons will be thermalized.

All three design options utilize boron in some form in the outer part of the shield, but they differ in the compounds and distribution of boron. In one concept, borated steel is used, with boron representing 0.8%. The slightly steeper decrease of the neutron flux above 0.1 MeV, as indicated in Fig. X-5 for Option 2 and in Fig. X-6 for Option 3, suggests that a wider boron-steel/water region will reduce the neutron flux at the outer boundary of the shield. This solution is attractive regarding neutronics, but its main potential disadvantage relates to the lower mechanical properties of borated steel. The penalty of using borated steel depends on how much stainless steel is used in the shield for structural purposes.

In another concept, boron carbide is laminated with alternate stainless steel layers. Calculations [4] showed a reduction in the magnet dose by using boron carbide.

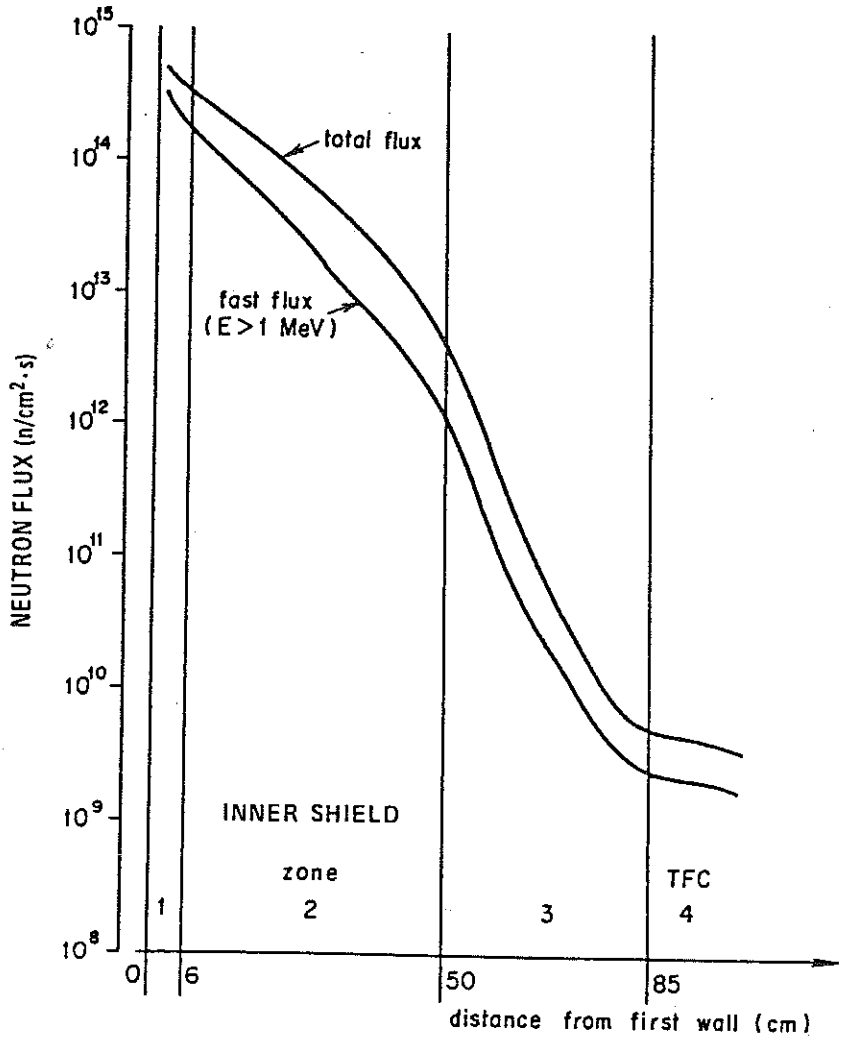

FIG. X-6. Neutron flux attenuation in the 85-cm-thick inner shield.

The boron-steel/water structure was employed as a reference design because of a possibly simpler and less costly structure compared with a B_4C structure.

In the reference design, the shield region is divided into two regions of 40 cm each (see Chapter IV for the engineering aspects; the first region contains 90% SS 316 and 10% H_2O, the second region contains boron-steel and water. A gap must be provided between the two shield regions. A detailed neutronics analysis will be required for the reference configuration, but analyses show that the three design options meet the shield requirements. The reference configuration is illustrated in Fig. X-4.

TABLE X-4. RADIATION RESPONSE PARAMETERS IN THE INBOARD TOROIDAL FIELD COILS

Based on 1.3 MW/m^2 neutron wall loading and 6 $MW \cdot a/m^2$ neutron exposure

Maximum neutron fluence in the superconductor ($E > 0.1$ MeV)	3.88×10^{17} n/cm^2
Maximum induced resistivity in the copper stabilizer	3.1×10^{-8} $\Omega \cdot cm$
Maximum atomic displacement in the copper stabilizer	2.54×10^{-4} displacements per atom
Maximum nuclear heating in the superconductor	
Neutron	0.92×10^{-5} W/cm^3
Gamma	8.24×10^{-5} W/cm^3
Total	9.16×10^{-5} W/cm^3
Nuclear heating in the superconductor and TF case	
Neutron	0.35 W/cm
Gamma	6.86 W/cm
Total	7.21 W/cm
Nuclear heating in the superconductor, TF case and dewar	
Neutron	0.62 W/cm
Gamma	16.10 W/cm
Total	16.72 W/cm
Dose in the thermal insulator	
Neutron	1.6×10^9 rad
Gamma	0.9×10^9 rad
Total	2.5×10^9 rad
Dose in the electrical insulator	
Neutron	5.1×10^8 rad
Gamma	1.7×10^8 rad
Total	6.8×10^8 rad

3.1.2. Neutronics calculations and results

For Design Option 1, a parametric analysis of the homogeneous one-dimensional model was performed in order to find the optimum material composition of steel, H_2O and B_4C that minimizes nuclear heating and neutron fluence in the superconducting toroidal field coils, radiation-induced resistivity and atomic displacement in the stabilizer, and radiation dose in thermal and electrical insulators. The analysis gives an optimum homogeneous composition of 80% Fe-1422, 10% B_4C and 10% H_2O. This homogeneous composition was used to guide the heterogeneous calculations. A series of calculations resulted in defining the configuration shown in Fig. X-4 as Design Option 1. This configuration results in the radiation response parameters shown in Table X-4. The maximum neutron fluence is below the reported damage threshold for the Nb_3Sn conductor by a factor of 2.5. The maximum induced resistivity in the copper stabilizer is 3.1×10^{-8} $\Omega \cdot$cm and it decreases very fast with distance into in the TF coils. The maximum dose in the thermal insulator is 1.6×10^{9} rad, which is well below the acceptable limit. The maximum nuclear heating in the superconductor is 9×10^{-5} W/cm^3, which does not cause any design difficulty for the TF coils. Thus, Design Option 1 meets all of the design criteria. The results shown in Table X-4 are based on the analyses for the case of a carbon armour. However, the shield performance is improved with the reference steel armour.

In Design Option 2, the calculations were made according to the MOSDIF and ANISN programs. The neutron flux for $E > 0.1$ MeV was obtained as a function of shield thickness at the optimum percentage of stainless steel and water (Fig. X-7). The fluence values in Fig. X-7 are normalized to a first-wall 14 MeV neutron flux density of 5.76×10^{13} n/cm$^2 \cdot$s at a total operation time of 10^8 s (note that the INTOR life is $\sim 1.45 \times 10^8$ s). The neutron flux density at $E > 0.1$ MeV is equal to 2.3×10^{14} n/cm$^2 \cdot$s. Using a neutron fluence of 5×10^{17} n/cm^2 at $E > 0.1$ MeV as an allowable value, the required shield thickness is less than 80 cm. At this thickness, the optimum percentages of steel and water are 73% and 27%, with the energy release in the superconducting coils of the order of several kilowatts.

For Design Option 3, the fast neutron flux and the total flux through the shield are shown in Fig. X-6.

The fast neutron flux density at the TF coils is about 2×10^{9} cm$^{-2} \cdot$s^{-1}, and the fluence at the end of life is about 2×10^{17} cm^{-2}.

3.2. Outboard bulk shield

3.2.1. Shield configuration

The outboard shield should meet the criteria for personnel access as well as those for the protection of superconducting coils. The allowable space for the

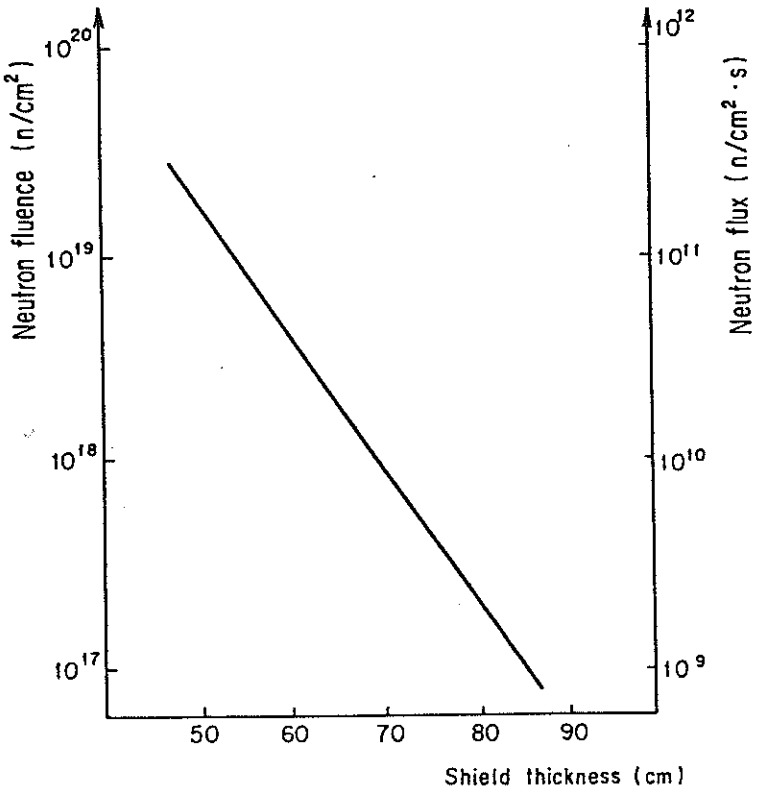

FIG.X-7. Neutron flux and fluence ($E > 0.1$ MeV) as a function of the shield thickness for optimum stainless steel concentration (balanced by H_2O).

outboard region, including first wall, blanket, shield and gaps, is 1.65 m (see Section IV-4), and the actual shield thickness should be less than 105 cm so as to keep 10 cm for the gap between the blanket and the shield.

Four outboard shield configurations were examined and compared (see Fig. X-8) [2–5]. In all configurations, steel (which has a high density) is used as the main shield material in the region next to the blanket. Two configurations employ boron steel (0.8% B) in the neutron absorption region and the other two use B_4C with a lead layer for gamma shielding. All four concepts have an actual shield thickness of less than 100 cm.

Boron steel has been chosen as neutron absorber in the reference design, as for the inboard shield. However, B_4C can be used alternatively, with more detailed calculations to be performed in Phase One.

The requirement for a thicker shield based on a three-dimensional analysis (see Section 4) leads to the 105-cm-thick shield that is recommended for the reference configuration.

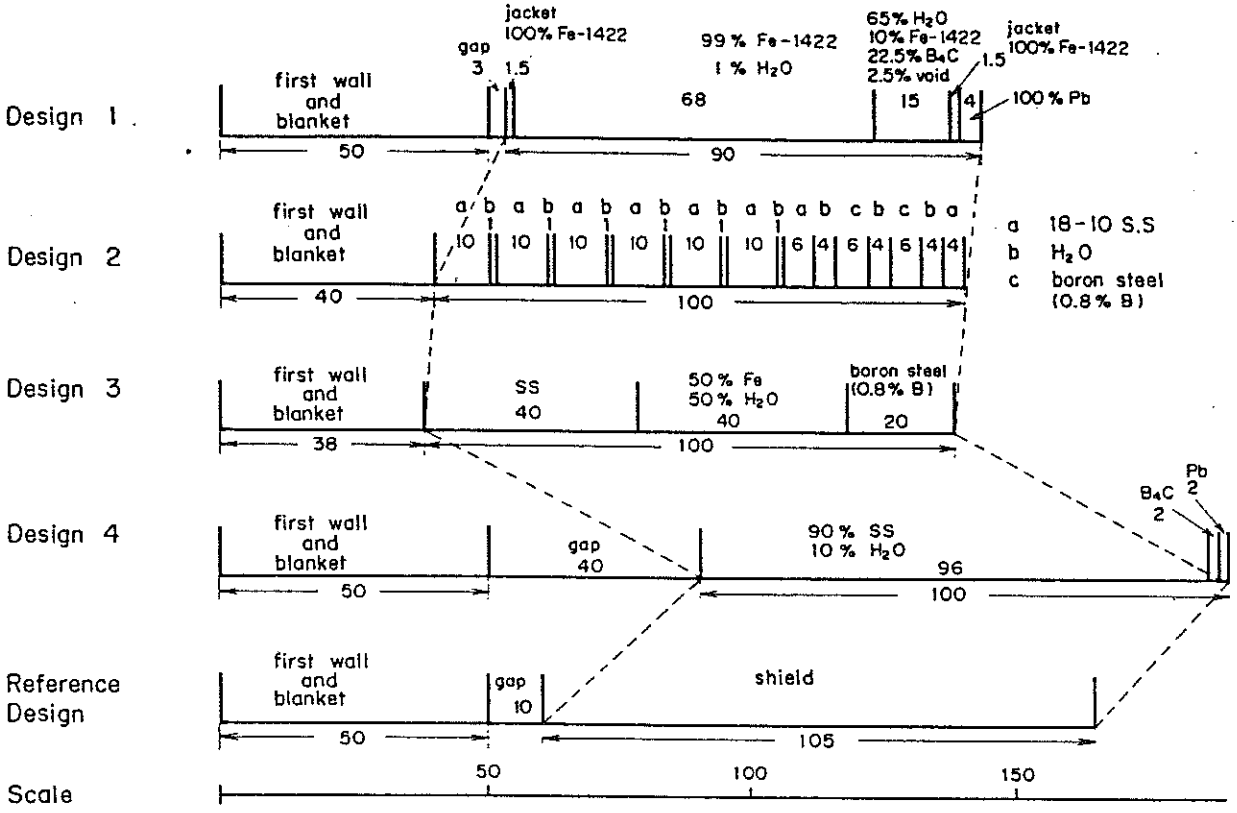

FIG.X-8. Comparison of design options for outboard shield configuration. (Dimensions in cm)

Region	Thickness (cm)	Material
1	1.5	100% Fe-1422 (jacket)
2	70	90% Fe-1422
		10% H_2O
3	28	65% boron-steel
		(or 45% Fe-1422 + 15% B_4C
		+ 35% H_2O)
4	1.5	100% Fe-1422 (jacket)
5	4	100% Pb
Total	105	

A 10 cm gap is kept between the blanket and the shield (see Fig. X-8).

3.2.2. Neutronics calculations and results

In addition to radiation protection of reactor components, the outboard shield is critical in satisfying personnel access requirements. The biological dose

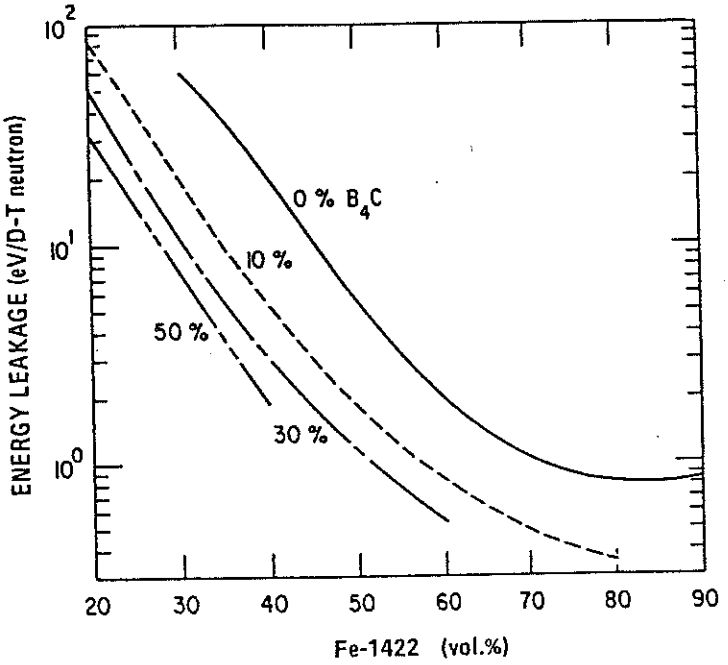

FIG. X-9. Energy leakage per fusion neutron from the outboard shield as a function of the Fe-1422 concentration in the outboard shield for different boron carbide concentrations.

rate in the reactor building outside the bulk shield should be < 2.5 mrem/h at 24 hours after shut-down, with all shielding in place. Satisfying the personnel access criterion requires that (a) the bulk and penetration shields be effective in significantly reducing the neutron flux at the exterior reactor components, and (b) the materials in the outermost region of the exterior components (including the outer region of the bulk and penetration shields) do not produce strong decay gamma rays.

In Design Option 1, as a process for optimization, an initial analysis was carried out for a 0.9-m-thick shield, with a mixture of Fe-1422, B_4C and H_2O, in a homogeneous model at the reactor mid-plane. The results were used as input for heterogeneous analyses. The minimum energy leakage from the outboard shield components occurs with a mixture of 80% Fe-1422, 10% B_4C and 10% H_2O, as shown in Fig. X-9. The neutron energy leakage is 0.18 eV per D-T neutron and shows a small dependence on B_4C concentration, while the gamma-ray energy leakage is a factor of four more than without B_4C. It is important to reduce the reaction rates of $^{55}Mn(n, 2n)^{54}Mn$ and $^{58}Ni(n, p)^{58}Co$.

Optimization for different heterogeneous material arrangements was performed in a manner similar to that used for the inboard shield. With the B_4C region at the outer location, the neutron leakage is reduced by a factor of two compared with the case of a homogeneous distribution.

TABLE X-5. RADIOISOTOPES CAUSING MORE THAN 90% OF THE RADIATION DOSE AT 24 HOURS AFTER SHUT-DOWN AND THE NEUTRON INTERACTIONS PRODUCING THEM

Isotope	Neutron interactions
^{51}Cr	$^{54}Fe(n,n'\alpha)^{51}Cr$
	$^{52}Cr(n,2n)^{51}Cr$
^{54}Mn	$^{55}Mn(n,2n)^{54}Mn$
	$^{54}Fe(n,p)^{54}Mn$
	$^{56}Fe(n,t)^{54}Mn$
^{57}Co	$^{58}Ni(n,d)^{57}Co$
^{58}Co	$^{60}Ni(n,t)^{58}Co$
	$^{58}Ni(n,p)^{58}Co$
^{99m}Tc	$^{98}Mo(n,\gamma)^{99}Mo \xrightarrow{\beta'} {}^{99m}Tc$

Special attention is given to neutron leakage with energies above 0.7 MeV, since this part of the neutron spectrum causes more than 90% of the radiation dose at 24 hours after shut-down. Table X-5 lists these radioisotopes and the neutron interactions producing them. ^{58}Co causes more than 50% of the radiation dose from Type 316 stainless steel at 24 hours after shut-down and is produced from ^{58}Ni through the reaction $^{58}Ni(n, p)^{58}Co$, with 0.7 MeV neutron threshold energy.

Figure X-10 compares the neutron flux for the homogeneous distribution with Design Option 1, for which the flux has a lower value for $E > 0.7$ MeV. The neutron fluence for Design Option 2 is shown in Fig. X-11.

In the analysis for Design Option 4 [3, 10], only a homogeneous model is studied because multi-layers of SS and water are not considered very effective in reducing the induced radioactivity outside the shield. This is based on the fact that the major sources of the gamma-ray dose rates after shut-down are the products of the (n, p) reactions from the 14 MeV neutrons, i.e. ^{58}Co and ^{54}Mn, when SS 316 is used.

Values for induced activity and gamma-ray dose rates after shut-down are obtained using the THIDA code system [11], which calculates Transmutation, Hazard potential, Induced activity, Dose rate and Afterheat. This system consists of a calculation code for induced activity and data libraries of activation reaction

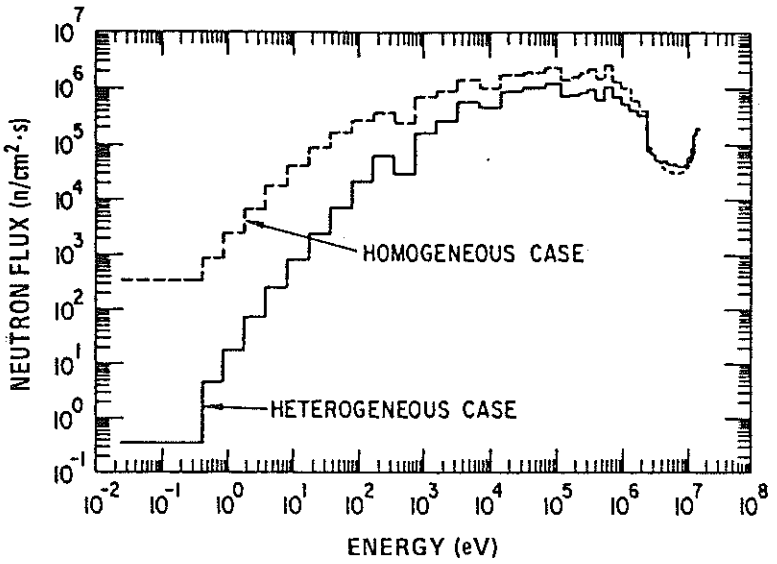

FIG.X-10. Neutron flux at the outboard shield boundary for the homogeneous distribution and for Design Option 1 (final design).

cross-sections, activation chains, radionuclide gamma-ray energy/intensity, gamma-ray transport cross-section and flux-to-dose conversion factors. The transport calculation of neutrons is done with the ANISN code [12] and the coupled 42-group gamma-ray cross-section set GICX 40 [13]. The transport of shut-down gamma-rays is also calculated with ANISN and a 54-group gamma-ray cross-section set included in the THIDA system [11]. The P_5-S_8 approximation is used in the transport calculations. The calculation results for induced activity of Design Option 4 are presented in the next section.

3.2.3. Biological dose rate after shut-down

One of the most important design criteria for the outboard shield is that the biological dose rate must be kept as low as possible for reactor maintenance. The dose rate should be less than 2.5 mrem/h at 24 hours after shut-down on the outer surface of the outboard shield.

For Design Option 4, the induced activity for the whole reactor after two years of continuous operation is shown in Fig. X-12 as a function of time after shut-down. The total induced activity at reactor shut-down is 7×10^8 Ci for a fusion power of 600 MW, i.e. about 10^6 Ci/MW.

In Design Option 4, after 2 years of continuous operation, most of the dominant isotopes, except ^{54}Mn (with a half-life of 313 days), ^{57}Co (727 days) and ^{60}Co (5.27 years), have reached the respective saturation activity. The spectra

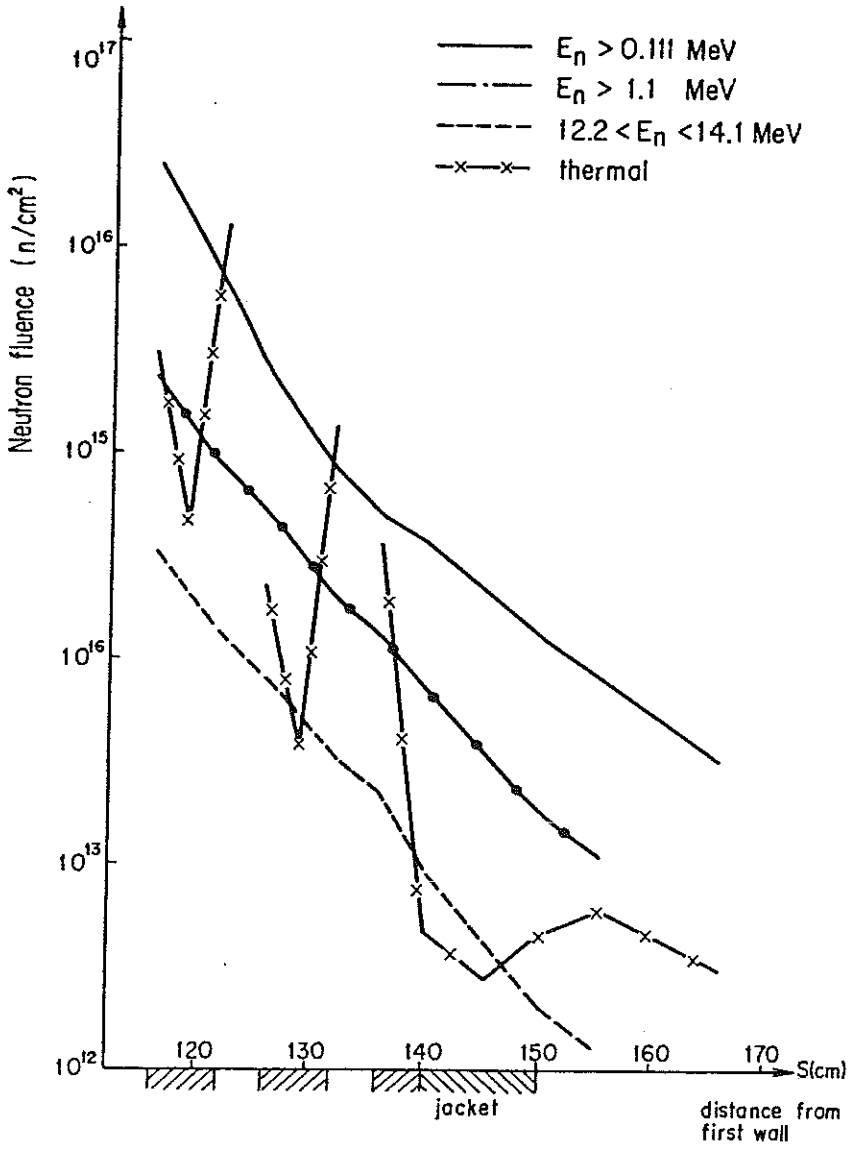

FIG. X-11. Neutron fluence for Design Option 2 (outboard shield).

of decay gamma rays, one day after shut-down, at three locations, are shown in Fig. X-13. The peaks of ^{60}Co and ^{57}Co gamma rays are more pronounced at the first wall. A comparison of the neutron spectra in front of B_4C and the lead layer, and at the magnet dewar clearly shows the effectiveness of ^{10}B absorption of low-energy neutrons which resulted in reducing the peaks of ^{59}Fe and ^{51}Cr. Figure X-14 shows specific induced activities of ^{58}Co, ^{54}Mn, ^{59}Fe and ^{51}Cr in the components of Design Option 4, at 24 hours after shut-down.

For Design Option 1, radiation dose analyses were performed in two steps. The first step utilized a one-dimensional model (no penetrations) to identify the

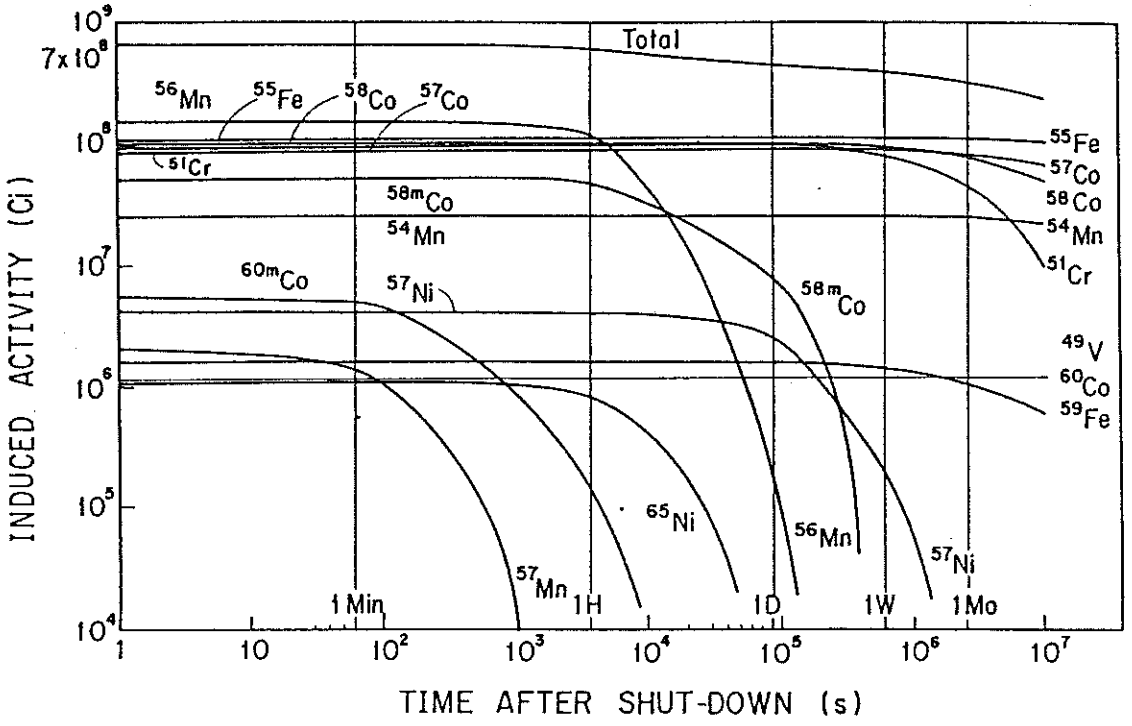

FIG.X-12. Induced activity for the whole reactor as a function of time after shut-down (total induced activity and induced activity of each radionuclide).

performance and requirements of the bulk shield. The second step was based on a three-dimensional model to analyse the whole reactor and to check the compliance with the design specifications.

In the one-dimensional calculations, the neutron transport as well as the decay gamma transport are solved by ANISN [12], based on an infinite cylinder model. Radioactivity and its related parameters such as decay gamma yield and decay afterheat are calculated by an activation code, RACC [14] together with the associated data libraries of RACCXLIB and RACCDLIB [15]. For dose analysis, flux-to-dose conversion factors presented in Ref. [16] have been used.

The low nickel content in Fe-1422 substantially reduces the production of a series of short-lived cobalt isotopes, in particular ^{58}Co (half-life 71 d). At about 24 hours after reactor shut-down, a large fraction of the short-term activation in the relatively high-nickel steel is caused by the ^{58}Co isotope resulting from the reaction ^{58}Ni(n, p)^{58}Co. The low nickel content in Fe-1422 reduces not only the short-term activation but also the long-term activation, reflecting the reduced ^{63}Ni production resulting from the reaction ^{62}Ni(n,γ)^{63}Ni. ^{63}Ni (half-life ~ 100 years) is the most dominant source of the long-term activation after decay of the ^{55}Fe

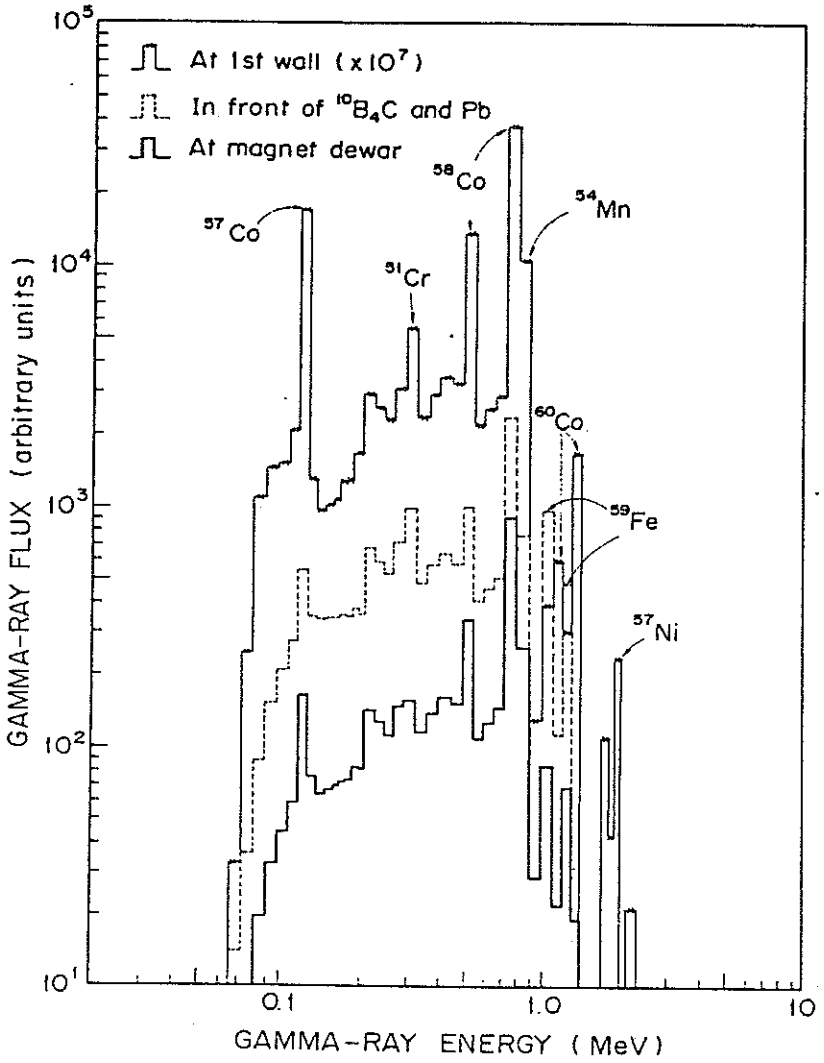

FIG.X-13. Gamma-ray spectra, one day after shut-down, at three locations – Design Option 4. (The spectrum at the first wall is to be multiplied by 10^7.)

activity and until the activity of the impurity elements such as ^{14}C becomes significant. Of primary concern regarding the high manganese content in Fe-1422 is the potential increase in the short-term production of ^{56}Mn (2.6 h) and the long-term production of ^{53}Mn (3.7×10^6 a) and ^{54}Mn (312 d).

Table X-6 shows the radioactivity concentration in the outboard shield of Design Option 1 for post-shut-down times. The largest part of the shield (Shield 1) contains mostly Fe-1422 in order to enhance the neutron energy moderation by inelastic reactions. This iron-rich shield design is based on considerations of minimizing short-term activation which is mostly caused by high-energy neutron

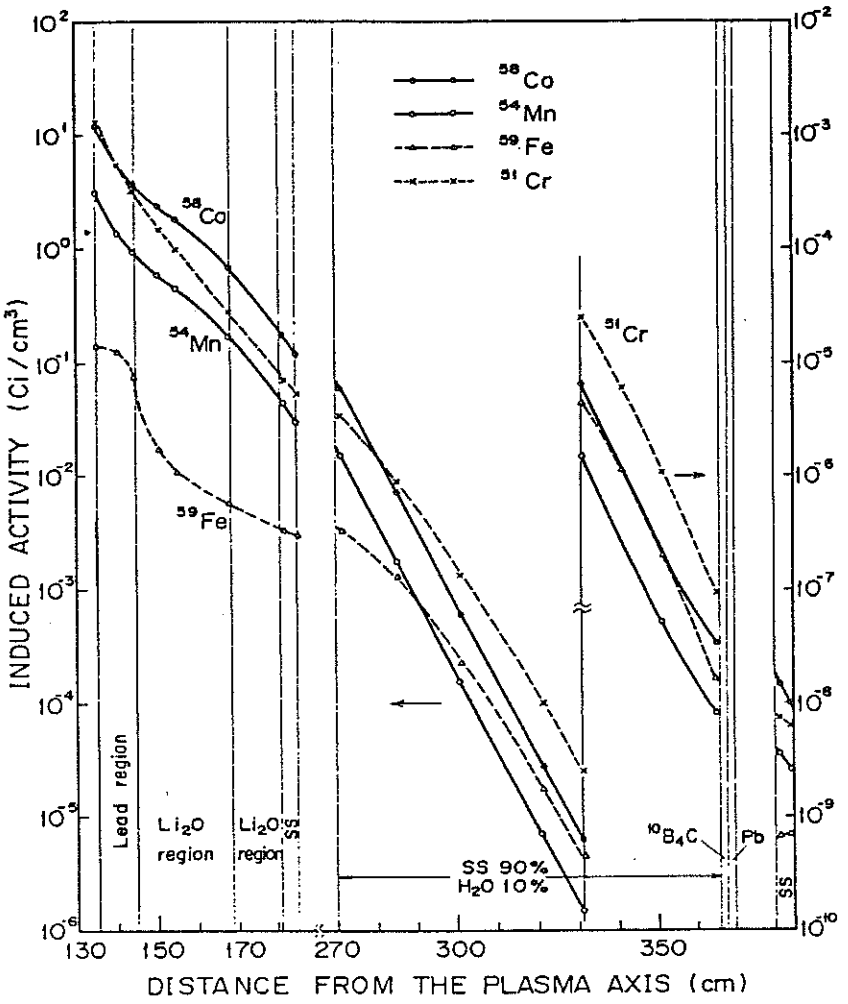

FIG.X-14. Specific induced activities of ^{58}Co, ^{54}Mn, ^{59}Fe and ^{51}Cr in the blanket, shield and magnet dewar of Design Option 4, at 24 hours after shut-down.

interactions such as $^{58}Ni(n, p)^{58}Co$. As a result, the population of low-energy neutrons is relatively high in this system, as shown below. The relatively slow decrease of radioactivity over a period of 0–10 years is caused by ^{55}Fe (2.7 a). After this period and up to about 100 years, the activation level drops sharply, reflecting ^{55}Fe decay, and then follows another slow activation decrease due to ^{63}Ni. Most of the shield materials are likely to be classified as medium-level wastes, with 10^{-4} to 10 kCi/m^3, within one year after shut-down.

The contact biological dose rate for this 90-cm-thick shield is higher than the design criterion of 2.5 mrem/h at about 24 hours after shut-down, as shown in Table X-7. When the shield thickness is increased to 105 cm, the biological dose rate at 24 hours after shut-down is < 1 mrem/h, according to one-dimensional calculations.

TABLE X-6. RADIOACTIVITY CONCENTRATION IN THE OUTBOARD BULK SHIELD (DESIGN OPTION 1)

Component	Thickness (cm)	Composition	MCi/m^3			
			Time after shut-down			
			0	24 h	1 a	100 a
Inner shield jacket	1.5	Fe-1422	5.2(0)[a]	5.9(−1)	3.5(−1)	6.8(−5)
Shield-1						
-1A	17.0	99% Fe-1422 + 1% H_2O	1.4(0)	1.7(−1)	1.0(−1)	2.7(−5)
-1B	17.0		3.2(−1)	1.3(−2)	7.6(−3)	5.2(−6)
-1C	17.0		8.3(−2)	1.6(−3)	8.9(−4)	1.4(−6)
-1D	17.0		1.6(−2)	2.2(−4)	1.1(−4)	2.8(−7)
Shield-2						
-2A	7.5	10% Fe-1422 + 65% H_2O + 22.5% B_4C	1.9(−4)	1.6(−6)	7.4(−7)	1.4(−9)
-2B	7.5		9.7(−6)	2.4(−7)	1.3(−7)	8.2(−10)
Outer shield jacket	1.5	Fe-1422	1.9(−5)	1.2(−6)	6.6(−7)	1.8(−10)
Lead cover	4.0	Pb	3.9(−8)	2.9(−8)	7.0(−14)	7.0(−14)
Magnet dewar	10.0	Type 304 SS	1.2(−6)	4.1(−7)	1.5(−7)	5.8(−10)

[a] Read as 5.2×10^0.

TABLE X-7. CONTACT BIOLOGICAL DOSE RATE (rem/h) FOR OUTBOARD BULK SHIELD (DESIGN OPTION 1)

	Time after reactor shut-down		
	0	1 day	1 week
End of shield	2.4	0.060	0.055
Magnet dewar surface	1.8	0.053	0.048

As a second step for Design Option 1, a three-dimensional dose analysis was performed, in order to satisfy the 2.5 mrem/h dose-rate limit on the outer surface of the bulk shield at 24 hours after shut-down. The neutron fluxes obtained from the three-dimensional neutron transport calculation were used to generate a gamma source at 24 hours after shut-down in every reactor zone. Using this gamma source, a gamma transport calculation was carried out to obtain the gamma flux, gamma heating and radiation dose at several locations of the reactor. The geometrical model used for the neutron transport was also used for the decay gamma transport (see Section 4).

Three-dimensional analyses indicate that the bulk shield thickness must increase to 105 cm instead of 90 cm and the thickness of the penetration shields must be greater than certain values, as discussed in Section 4.

4. PENETRATION SHIELDS

In order to perform the penetration shield analysis for the neutral beam injectors and the divertor system for the INTOR design, elaborate calculations were carried out in Ref. [4] in great detail, assessing the impact on reactor operation and accessibility after shut-down. A three-dimensional model describing the details of the reactor system was used in the analysis. The general-purpose Monte-Carlo code MCNP [17] was used for the calculations. A continuous energy representation for the nuclear cross-section from ENDF/B-IV was employed for the calculations. The energy spectrum and the spatial distribution of the D-T source neutrons were considered in the analysis. Calculations of coupled neutron and neutron-induced photon transport during operation, and of decay photon transport after shut-down were performed using the same geometrical model. The calculations were made for an earlier version of the design, which is slightly different from the present reference design, but the conclusions are still applicable.

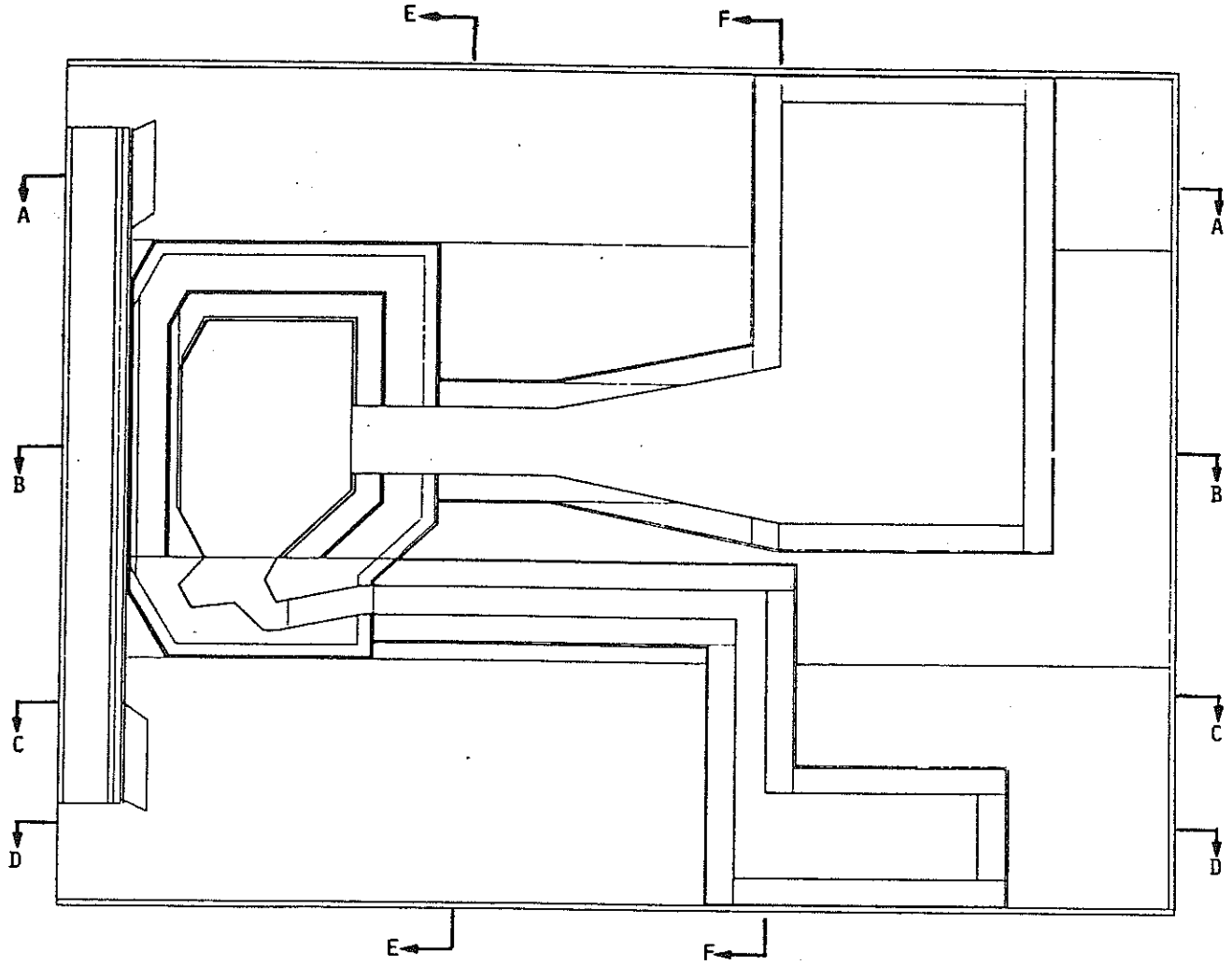

FIG.X-15. Vertical cross-section of the three-dimensional geometrical model used for the shielding analysis between two toroidal field coils, showing the blanket, shield, neutral beam and divertor.

4.1. Geometrical model and calculation method

The three-dimensional geometrical model shown in Figs X-15 to X-18 describes the whole reactor, the different components of which are represented explicitly in the model. The reactor parameters used in the model are listed in Table X-8. The model makes use of the reactor symmetry (12 toroidal field coils, 6 neutral beam injectors, 12 divertor ducts) by considering a 30-degree sector which includes one TF coil, one divertor duct, and one-half neutral beam injector, as shown in Figs X-15 to X-18.

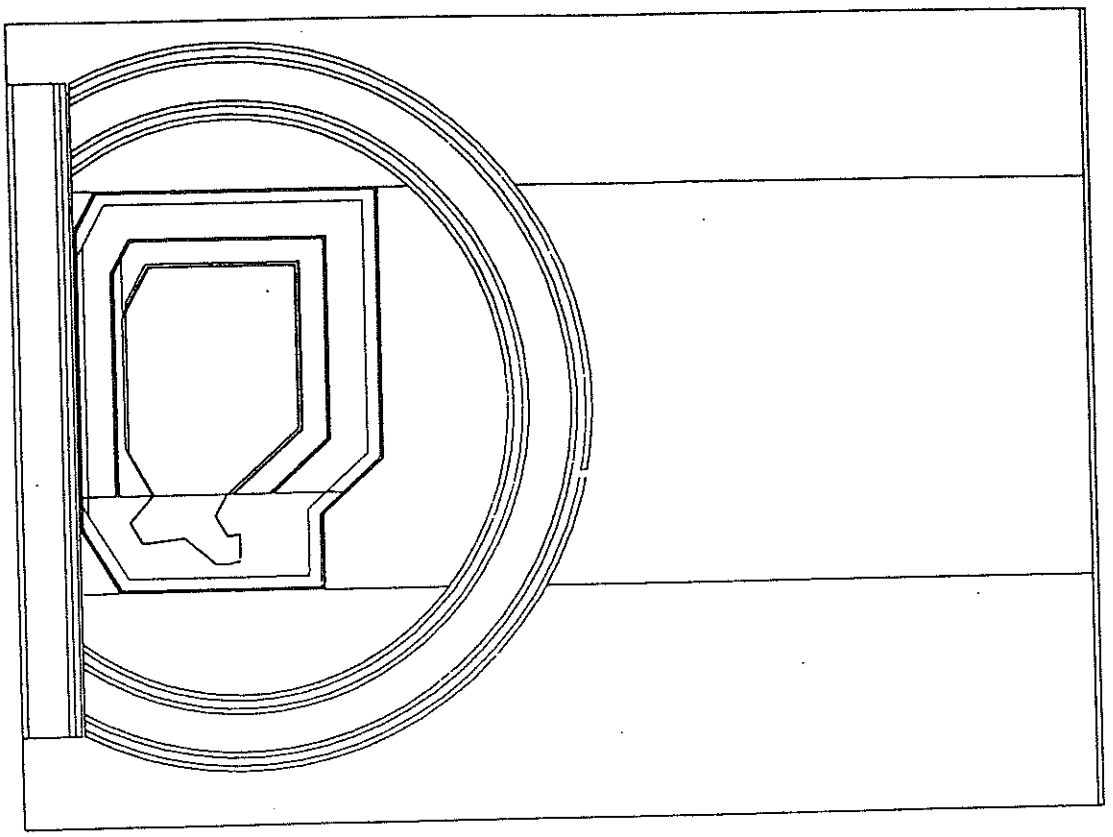

FIG. X-16. Vertical cross-section of the three-dimensional geometrical model used for the shielding analysis, showing the blanket, bulk shield and one toroidal field coil.

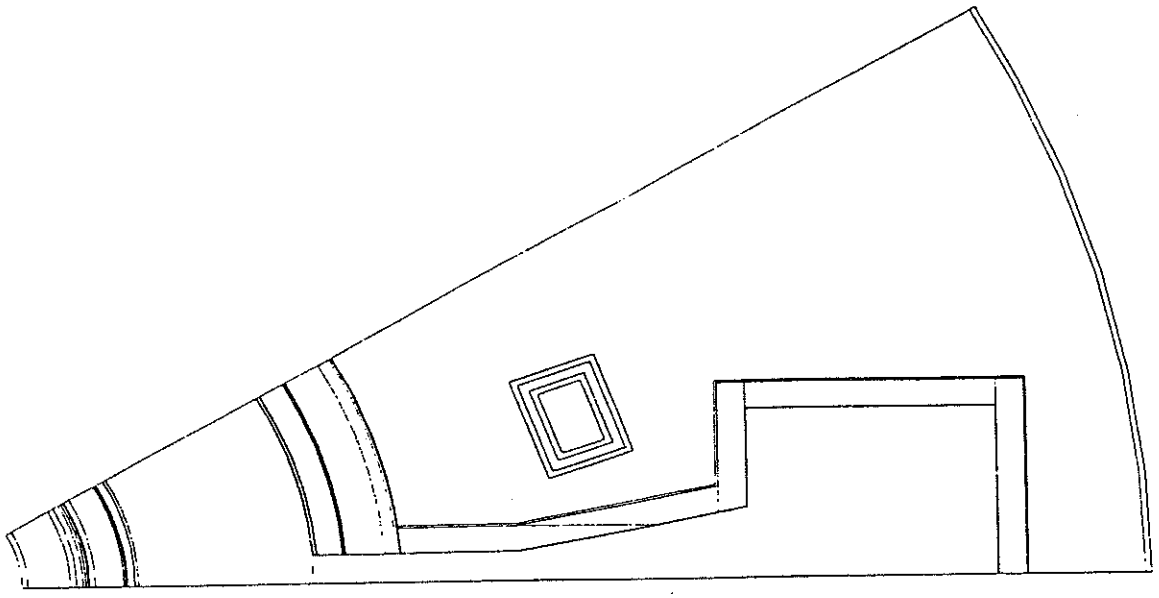

FIG. X-17. Section B–B (Fig. X-15) of the three-dimensional geometrical model used for the shielding analysis.

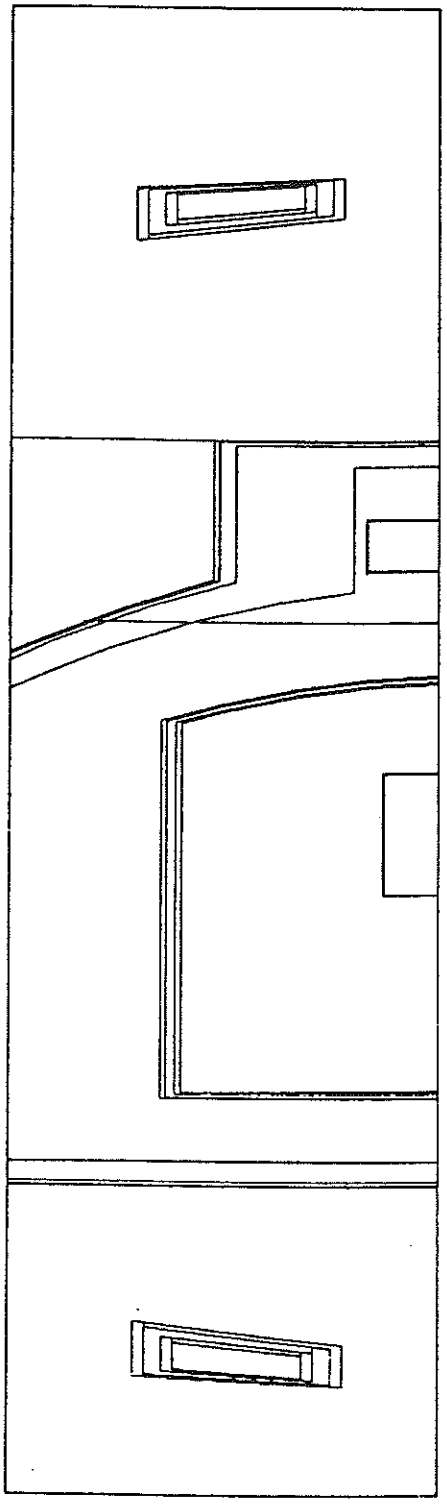

FIG.X-18. Section E–E (Fig.X-15) of the three-dimensional geometrical model used for the shielding analysis.

TABLE X-8. REACTOR PARAMETERS USED IN THE THREE-DIMENSIONAL SHIELDING ANALYSIS FOR THE INTOR DESIGN

Reactor chamber	
Chamber major radius	5.2 m
Plasma major radius (R_0)	5.3 m
Plasma chamber radius	1.4 m
Plasma radius (a_0)	1.2 m
Plasma elongation (K)	1.6 m
Toroidal field coils	
Number	12
Conductor material	Nb_3Sn
Stabilizer material	Cu
Structural material	Type 316 SS
Neutral beam injectors	
Number	6
Port size	1.2 m × 1.0 m
Divertor system	
No. of divertor ducts	12
Divertor duct dimensions	0.5 m × 1.3 m
Power	
Average neutron wall loading	1.3 MW/m^2
Fusion neutron power	494 MW

Tables X-9 and X-10 give the dimensions and material compositions for the blanket and bulk shield used in the three-dimensional analysis. The shield thickness and composition used around the NB drift tube, NB box, and divertor systems are shown in Table X-2.

The building liner is taken into account by including a 10 cm layer of Type 316 stainless steel.

The neutron source distribution described in Section 2 was used. Two-hundred and thirty surfaces were used to describe 74 zones representing the different components in the reactor.

TABLE X-9. INBOARD BLANKET AND SHIELD PARAMETERS USED IN THE THREE-DIMENSIONAL SHIELDING ANALYSIS FOR THE INTOR DESIGN

Zone	Zone thickness (cm)	Zone composition (vol.%)	
First-wall armour	5	100%	Carbon
First wall	1	70%	Type 316 SS
		30%	H_2O
Blanket material	12.5	90%	Fe-1422 alloy
		10%	H_2O
Blanket jacket	1.5	100%	Type 316 SS
Vacuum	3		Void
Shield jacket	1.5	100%	Type 316 SS
Fe shield	45	90%	Fe-1422
		10%	H_2O
B_4C shield	10	18%	Fe-1422
		10%	H_2O
		64.3%	B_4C
		7.2%	Void
Shield jacket	1.5	100%	Type 316 SS

The spatially distributed neutron source described in Section 2.4 is used for three-dimensional calculations.

4.2. Results and analysis

A coupled neutron and neutron-induced photon transport calculation with 10^5 D-T neutrons obtained sufficient statistical accuracy for the different reactor components.

For the purpose of calculation, the shield thicknesses around penetrations were selected to be smaller than those expected to be actually required. The reason was to reduce computer time and to obtain good statistical accuracy. The values can then be extrapolated to determine the required thicknesses, as discussed later.

TABLE X-10. OUTBOARD BLANKET (TRITIUM-BREEDING BLANKET) AND SHIELD PARAMETERS USED IN THE THREE-DIMENSIONAL SHIELDING ANALYSIS FOR THE INTOR DESIGN

Zone	Zone thickness (cm)	Zone composition (vol.%)	
First-wall armour	1	100%	Type 316 SS
First wall	1	70%	Type 316 SS
		30%	H_2O
Neutron multiplier	5	100%	Pb
Second wall	1	50%	Type 316 SS
		50%	H_2O
Tritium breeder	40.5	10%	Type 316 SS
		20%	H_2O
		42%	Li_4SiO_4
		28%	He
Blanket jacket	1.5	100%	Type 316 SS
Vacuum	3		Void
Shield jacket	1.5	100%	Type 316 SS
Fe shield	63	90%	Fe-1422 alloy
		10%	H_2O
Boron shield	20	20%	Fe-1422 alloy
		40%	H_2O
		36%	B_4C
		4%	Void
Pb shield	4	100%	Pb
Shield jacket	1.5	100%	Type 316 SS

Table X-11 gives the neutron and gamma heating in the different reactor components. A heat deposition of about 9 kW in the TF coils (TF case and superconductor) is obtained; the design specification sets a maximum of 5 kW. It should be noted that a penetration shield thickness of only 50 cm is used in the calculations; a small increase in thickness will reduce the total heat deposition in the TF coils to within the 5 kW limit. An additional penetration shield thickness

TABLE X-11. TOTAL NUCLEAR HEATING IN THE DIFFERENT REACTOR COMPONENTS

Zone	Neutron heating (MW)	Gamma heating (MW)	Total heating (MW)	Zone volume (m^3)
Reactor chamber				
Carbon armour	13.5	3.3	16.8	3.0
Steel armour	12.5	23.3	35.8	3.1
First wall	19.4	18.3	37.7	3.7
Neutron multiplier	36.2	26.8	73.0	14.3
Second wall	10.7	4.4	15.1	2.9
Tritium-breeding portion	189.0	34.0	233.0	126.3
Non-breeding portion	29.8	41.3	71.1	17.1
Blanket jacket	0.6	3.6	4.2	6.4
Inner shield jacket	0.5	3.0	3.5	6.6
Bulk shield	11.8	16.8	28.6	395.3
Outer shield jacket	8.8–3	3.3–2	4.2–2	8.4
Divertor chamber				
First wall	2.9	3.9	6.8	1.3
Shield	0.4	43.6	44.0	170.8
Shield jacket	5.2–3	5.4–4	5.7–3	3.6
Neutral beam				
Drift-tube surface	1.0	1.1	2.1	2.6
Drift-tube shield	5.1–2	2.9–2	8.0–2	124.2
Neutral-beam surface	2.3–2	3.8–2	6.1–2	11.6
Neutral-beam shield	3.4–1	2.3–1	5.7–1	671.6
Divertor duct				
Surface embedded in the bulk shield	4.2–2	1.3–1	1.7–1	0.3
Surface outside the bulk shield	4.5–3	1.8–2	2.3–2	3.6
Shield	9.1–2	3.8–2	1.3–1	270.2
Toroidal field coils				
Inner legs	2.4–4	3.1–3	3.3–3	165.6
Inner dewar	9.2–5	8.9–3	9.0–3	11.0
Outer legs	6.0–4	5.0–3	5.6–3	301.9
Outer dewar	1.3–3	1.1–2	1.2–2	161.3
Building liner				
Top section	4.2–5	4.8–4	5.2–4	125.8
Vertical section	2.1–4	9.6–4	1.2–3	185.1
Bottom section	1.1–4	1.9–4	3.0–4	125.8
TOTAL		562.71		

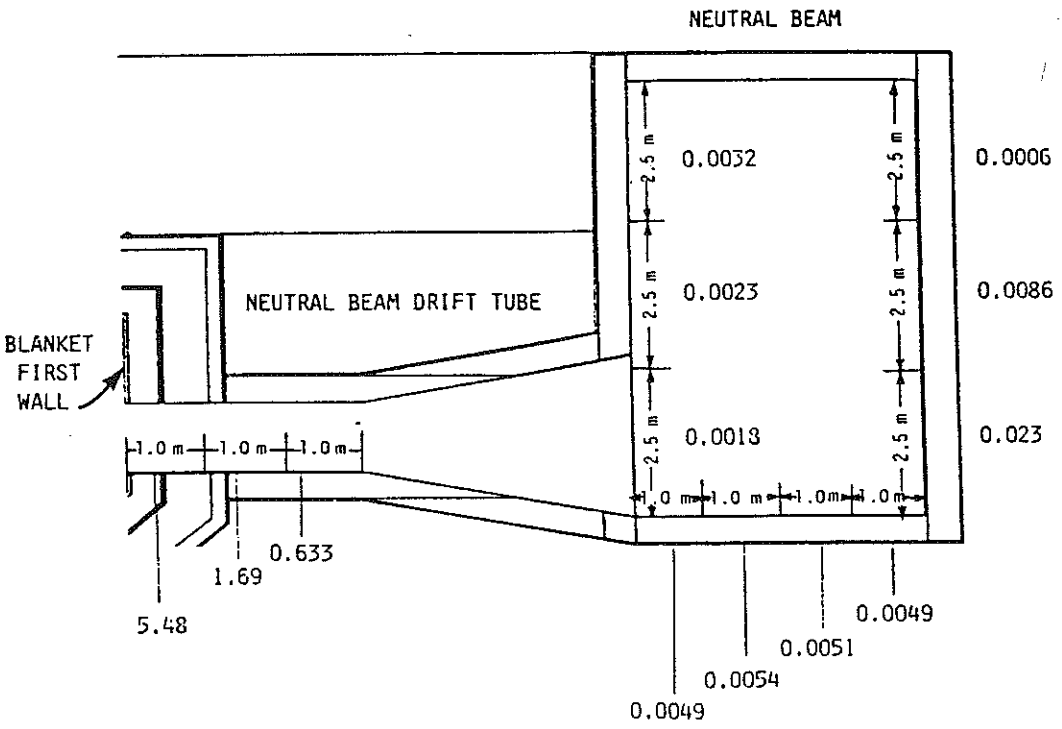

FIG.X-19. Neutral beam heating (W/cm^3).

of 15 cm around the neutral beam drift tubes will reduce nuclear heating in the outer portions of the TF coils by an order of magnitude, which results in about 4 kW heat deposition in the TF coils. However, the final penetration shield thickness around the neutral beam drift tubes is more than the 65 cm required for limiting nuclear heating in the TF coils and reducing the dose to personnel for access at 24 hours after shut-down.

Figure X-19 shows the nuclear heating in the surface (1 cm thick) of the neutral beam drift tube and the neutral beam injector box, averaged for different segments of the surface during the burn cycle, with the shutter open. The nuclear heating in the drift tube is averaged for 1 m segments starting from the first wall. The surface of the neutral beam box is divided into three parts: the first part faces the neutral beam drift tube and is perpendicular to the neutral beam drift tube axis; the second part is parallel to the first part but does not directly face the plasma; and the third part is the rest of the neutral beam box which consists of three surfaces parallel to the neutral beam drift tube. The maximum nuclear heating occurs in the area facing the plasma, as shown in Fig. X-19. The nuclear heating in the vacuum pumps located in the neutral beam boxes but not facing the plasma is ~ 3 kW at full neutron power, with the shutter open. Irradiation effects on components inside the beam injector box, such as magnet insulators and ion sources, are of concern and should be examined. Nuclear heating in the vacuum pumps of the divertor is less than 1 W, due to the long L-shaped duct (~ 14 m).

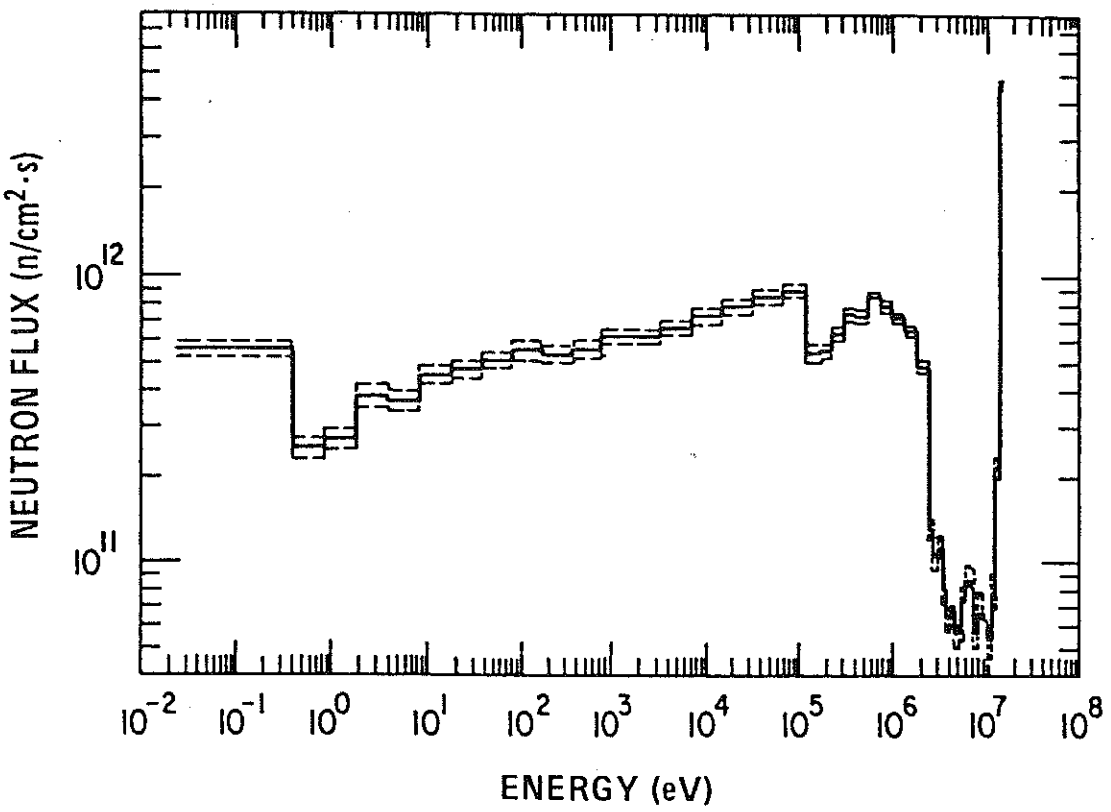

FIG.X-20. Average neutron flux in the neutral beam drift tube, normalized to 1.3 MW/m² neutron wall loading.

The total nuclear heating in the building liner is ~ 2 kW, with 6.5×10^{-6} W/cm³ maximum power density.

Figures X-20 to X-22 show the average neutron flux in the neutral beam drift tube, the neutral beam injector box and the reactor building, normalized to 1.3 MW/m² neutron wall loading. The dotted lines in the figures show the statistical errors of the calculations. The neutron flux outside the reactor shield obtained by three-dimensional analysis is two to three orders of magnitude greater than that obtained by one-dimensional analysis (see Fig. X-10). This increase is caused primarily by the neutral beam drift tube.

Figure X-23 gives the dose rate 24 hours after shut-down at the mid-plane and outside the shield in the reactor building. The maximum biological dose rate is 68.3 rem/h, as compared with 43.6 rem/h near the neutral beam drift tube. It should be noted that the dose near the drift tube is lower. The reasons for this are: (a) in the neutral beam drift tube, lead is used for the last layer of the shield (see Table X-10), which attenuates some of the decay gamma radiation from the shield around the neutral beam drift tube; and (b) the bulk shield jacket is of

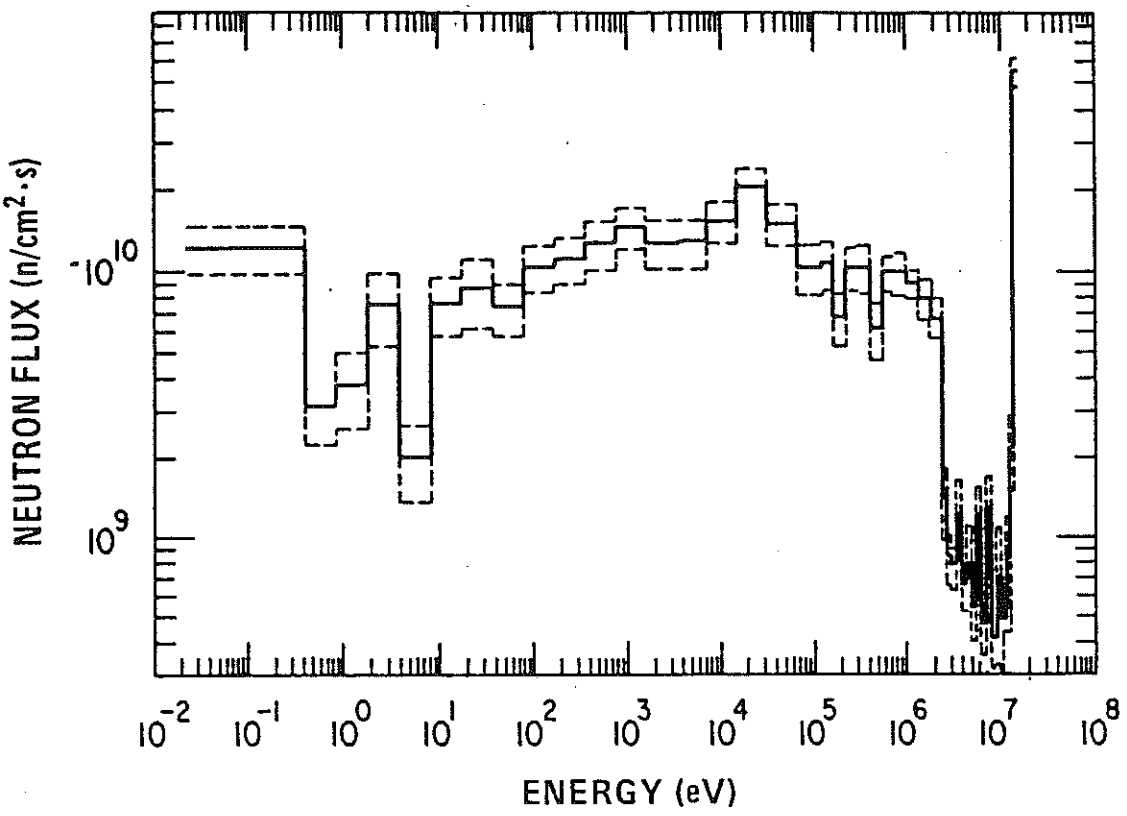

FIG.X-21. Average neutron flux in the neutral beam injector box, normalized to 1.3 MW/m² neutron wall loading.

Type 316 stainless steel (see Table X-2), the high nickel and chromium content of which contributes more to the dose. The one-dimensional analysis shows that the dose drops by a factor of two if the lead layer (4 cm) and steel jacket are interchanged.

Figure X-24 gives the dose rate in two vertical directions, which are indicated in Fig. X-23 by + signs. The first position is between two TF coils, the second behind the neutral beam system. The dose rate near the top and bottom corner of the reactor is influenced by the Type-316 stainless-steel reactor building liner, as shown in Fig. X-24.

According to one-dimensional analysis, the bulk shield thickness must be increased to 105 cm instead of 90 cm, in order to reduce the radiation dose rate in the reactor building to 2.5 mrem/h within 24 hours after shut-down. Extrapolating the neutron flux values from the three-dimensional analysis suggests the following shield thicknesses: (a) 100 cm for the neutral beam drift tubes; (b) 75 cm on the surfaces of the beam injector box facing the drift tubes; and (c) 50 cm for the rest of the neutral beam system and the divertor ducts.

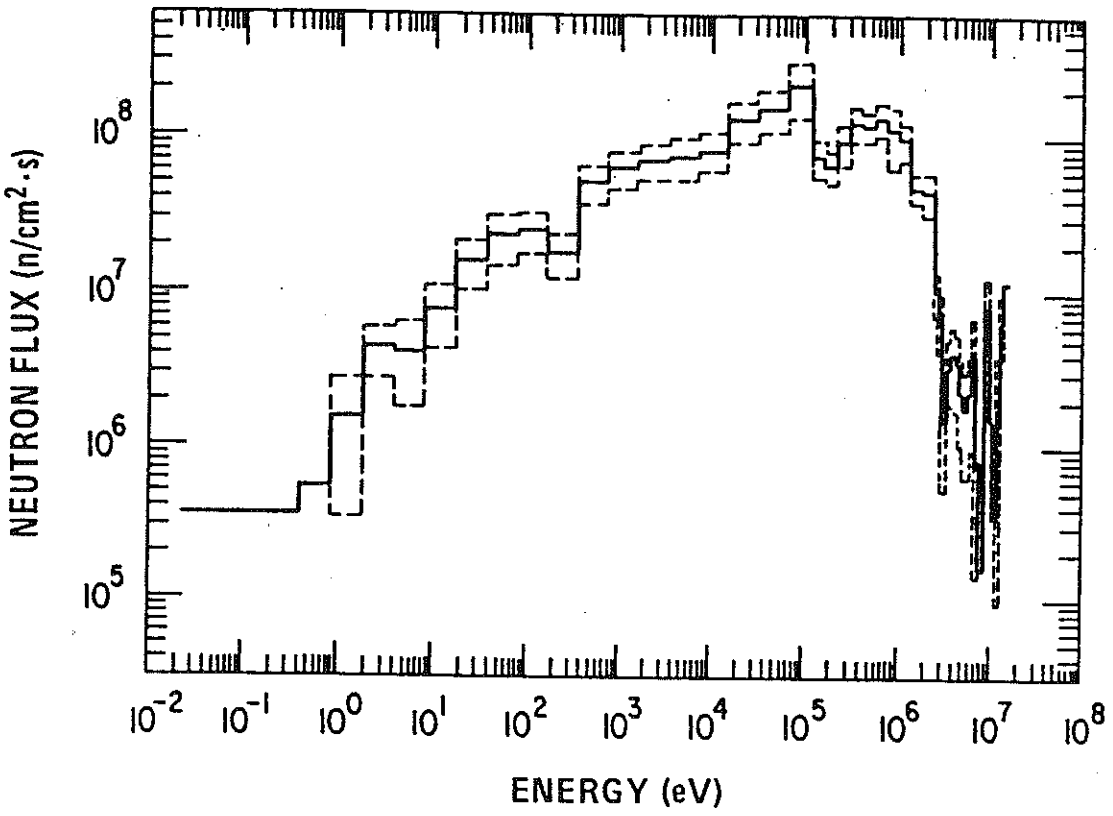

FIG.X-22. Average neutron flux inside the reactor building (outside the reactor shield), normalized to 1.3 MW/m² neutron wall loading.

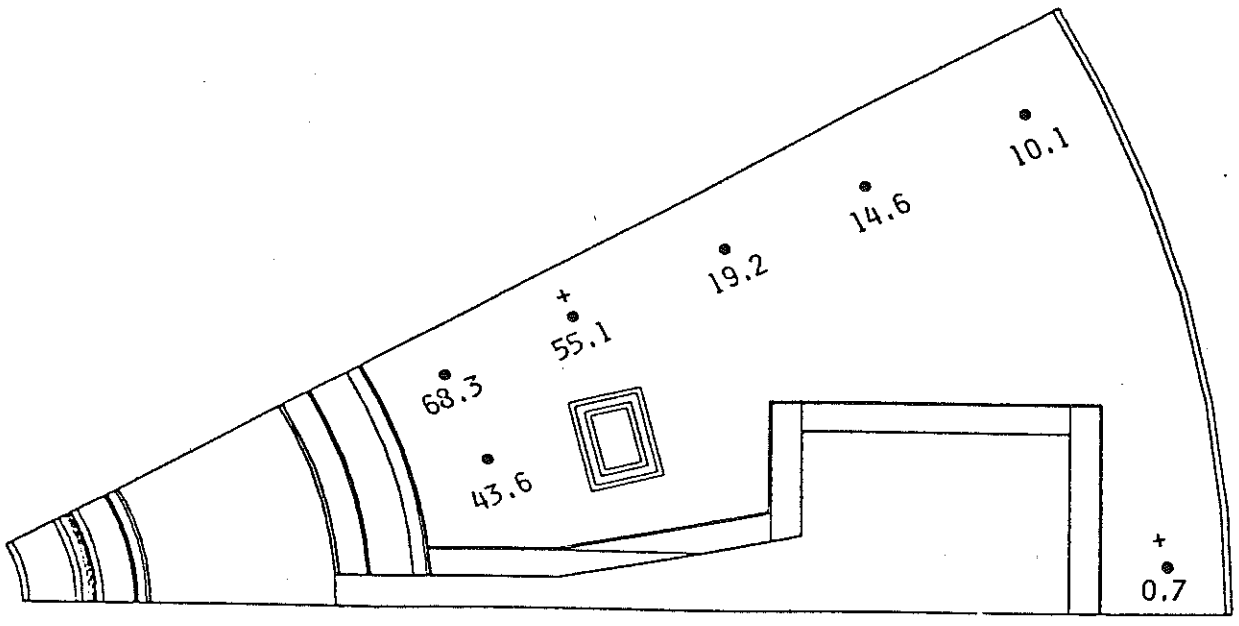

FIG.X.23. Dose rate (rem/h) at 24 hours after shut-down at the mid-plane.

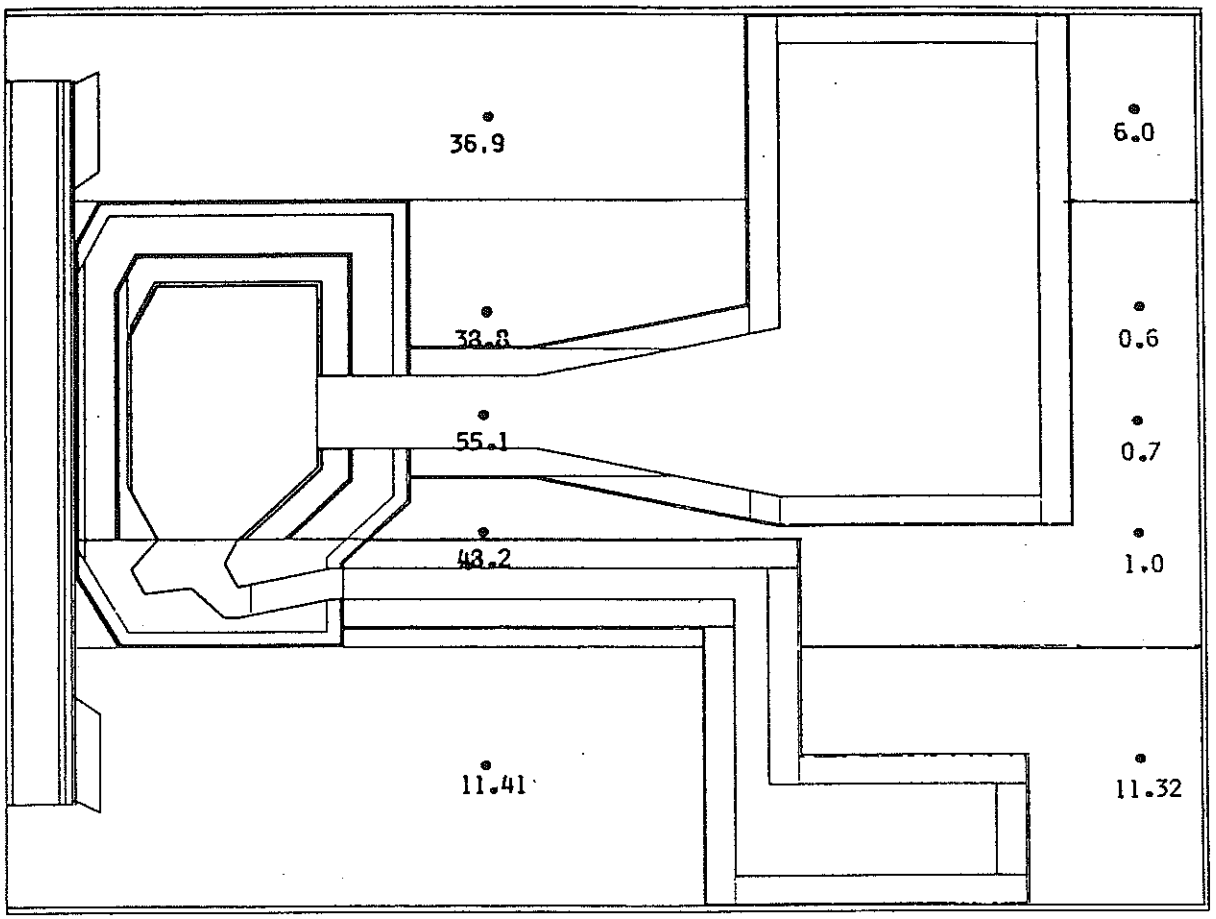

FIG.X-24. Dose rate (rem/h) at 24 hours after shut-down in two vertical directions.

5. GENERAL CONCLUSIONS

An actual thickness of 80 cm for a maximum allowable copper resistivity of $5 \times 10^{-8} \Omega \cdot$ cm is feasible for the torus inboard bulk shield. For the outboard bulk shield, a thickness of 105 cm is required in order to meet the criteria for personnel access.

For both bulk shields, the induced radioactivity can be lowered by the use of low-nickel steel.

The required thicknesses of the penetration shields are 100 cm around the neutral beam drift tube and 50 cm around the beam injector box. For special areas, exposed to radiation streaming, the shield thickness must be 75 cm. The thickness of the shield around the divertor duct is ~ 50 cm.

REFERENCES TO CHAPTER X

[1] INTOR GROUP, International Tokamak Reactor: Zero Phase (Rep. Int. Tokamak Reactor Workshop Vienna, 1979), International Atomic Energy Agency, Vienna (1980) 650 pp. *See also:* Summary in Nucl. Fusion 20 3 (1980) 349.

[2] Euratom Conceptual Design Contribution to the INTOR Phase-One Workshop, Rep. Commission of the European Communities, Brussels (1981).

[3] Japanese Conceptual Design Contribution to the INTOR Phase-One Workshop, Rep. Japan Atomic Energy Research Institute, Tokai-mura (1981).

[4] USA Conceptual Design Contribution to the INTOR Phase-One Workshop, Rep. INTOR/81-1, Georgia Institute of Technology, Atlanta, GA (1981).

[5] USSR Conceptual Design Contribution to the INTOR Phase-One Workshop, Rep. Kurchatov Institute, Moscow (1981).

[6] IIDA, H., et al., Poloidal Distribution of Neutron Flux Radial Damage and Nuclear Heating Rate in a First Wall System of INTOR-J, Rep. JAERI-M 8517, Japan Atomic Energy Research Inst., Tokyo (1979).

[7] Kobe Steel's Non-magnetic Steel Plate: NONMAGNE 30, Rep. No.A-78B20, Kobe Steel Ltd, Japan (1979).

[8] BAKER, C.C., et al., STARFIRE – a Commercial Tokamak Fusion Power Plant Study, Rep. ANL/FPP-80-1, Argonne National Lab., IL (1980).

[9] JUNG, J., ABDOU, M., Radioactive inventories and material recyclability in a tokamak reactor, Trans. Am. Nucl. Soc. 34 (1980) 645.

[10] SEKI, Y., IIDA, H., KAWASAKI, H., Fusion reactor shield optimization in terms of personnel access, J. Nucl. Sci. Tech. (to be published).

[11] IIDA, H., IGARASHI, M., THIDA – Code System for Calculation of the Exposure Dose Rate around a Fusion Device, Rep. JAERI-M 8019, Japan Atomic Energy Research Inst., Tokyo (1978) (in Japanese).

[12] ENGLE, W.W., Jr., A Users Manual for ANISN, a One Dimensional Discrete Ordinates Code with Anisotropic Scattering, Rep. K-1693, Computing Technology Center, Union Carbide Corporation (1976).

[13] SEKI, Y., IIDA, H., Coupled 42-Group Neutron and 21-Group Gamma Ray Cross Section Sets for Fusion Reactor Calculations, Rep. JAERI-M 8818, Japan Atomic Energy Research Inst., Tokyo (1980).

[14] JUNG, J., Theory and use of the radioactivity code, RACC, Rep. ANL/FPP/TM-122, Argonne National Lab., IL (1979).

[15] JUNG, J., Multigroup neutron activation cross section library RACCXLIB and decay data library, RACODLIB for the radioactivity calculation code, RACC (to be published).

[16] PROFIO, A.E., Radiation Shielding and Dosimetry, Wiley/Interscience, New York (1978).

[17] LASL Group X-6, MCNP-A General Monte Carlo Code for Neutron and Photon Transport, Rep. LA-7396-M, Los Alamos Scientific Lab., NM (Nov. 1979, Rev.).

PANEL PROCEEDINGS SERIES

INTERNATIONAL TOKAMAK REACTOR
Phase One

REPORT OF THE
INTERNATIONAL TOKAMAK REACTOR WORKSHOP
ORGANIZED BY THE
INTERNATIONAL ATOMIC ENERGY AGENCY
AND HELD IN SEVEN SESSIONS IN VIENNA
DURING 1980 AND 1981

INTERNATIONAL ATOMIC ENERGY AGENCY
VIENNA, 1982